9

# Insights into Phase Transformations from Mössbauer Spectroscopy

**Catherine A. McCammon**

*Bayerisches Geoinstitut*
*Universität Bayreuth*
*95440 Bayreuth, Germany*

## INTRODUCTION

The Mössbauer effect is the recoilless absorption and emission of γ-rays by specific nuclei in a solid (Mössbauer 1958a, 1958b), and provides a means of studying the local atomic environment around the nuclei. It is a short-range probe, and is sensitive to (at most) the first two coordination shells, but has an extremely high energy resolution that enables the detection of small changes in the atomic environment. Mössbauer spectroscopy therefore provides information on phase transformations at the microscopic level.

Mössbauer spectra of materials can be recorded under a large range of conditions, including temperatures from near absolute zero to at least 1200°C, and pressures to at least 100 GPa. Spectra can also be collected under different strengths of external magnetic field, currently to at least 15 T. This enables *in situ* observations of changes to the atomic environment before, during and after phase transformations under varying conditions. For phase transformations that are quenchable, it is possible to characterise changes between polymorphs at conditions where spectral resolution is optimal. Over 100 different Mössbauer transitions have been observed, although unfavourable nuclear properties limit the number of commonly used nuclei. The 14.4 keV transition in $^{57}$Fe is by far the most studied, and will be the focus of this chapter since iron is the most relevant nucleus for mineralogical applications.

The aim of this chapter is to provide a brief background to Mössbauer spectroscopy within the context of phase transformations. The relevant parameters are summarised and the effect of temperature and pressure are discussed, particularly with reference to identifying phase transformations and characterising the electronic and structural environment of the Mössbauer nuclei. Instrumentation is summarised, particularly as it relates to *in situ* measurements of phase transformations, and a brief survey of applications is given. The appendix includes a worked example that illustrates the methodology of investigating a phase transformation using *in situ* Mössbauer spectroscopy. Numerous textbooks and review chapters have been written on Mössbauer spectroscopy, and a selection of the most relevant ones as well as some useful resources are listed in Table 1.

## MÖSSBAUER PARAMETERS

The interactions between the nucleus and the atomic electrons depend strongly on the electronic, chemical and magnetic state of the atom. Information from these hyperfine interactions is provided by the hyperfine parameters, which can be determined experimentally from the line positions in a Mössbauer spectrum. The following section gives only a brief description of the parameters themselves, since this information is widely available in the references listed in Table 1. The section focuses on the structural and electronic information available from the parameters, and on the influence of

1529-6466/00/0039-0009$05.00 DOI:10.2138/rmg.2000.39.09

**Table 1.** List of resources for Mössbauer spectroscopy.

| *Type* | *Reference* |
|---|---|
| Book | Bancroft, G.M. Mössbauer Spectroscopy. An Introduction for Inorganic Chemists and Geochemists. McGraw Hill, New York, 1973. |
| | Berry, F.J. and Vaughan, D.J. (eds.) Chemical Bonding and Spectroscopy in Mineral Chemistry, Chapman and Hall, London, 1986. See Chapter on Mössbauer spectroscopy in mineral chemistry, A.G. Maddock, p. 141-208. |
| | Cranshaw, T.E., Dale, B.W., Longworth, G.O. and Johnson, C.E. Mössbauer Spectroscopy and its Applications, Cambridge University Press, Cambridge, 1986. |
| | Dickson, D.P. and Berry, F.J. (eds.) Mössbauer Spectroscopy, Cambridge University Press, Cambridge, 1986. |
| | Gibb, T.C. Principles of Mössbauer Spectroscopy, Chapman and Hall, London, 1977. |
| | Gonser, U. (ed.) Mössbauer Spectroscopy, Topics in Applied Physics, Vol. 5, Springer-Verlag, Berlin, 1975. |
| | Greenwood, N.N. and Gibb, T.D. Mössbauer Spectroscopy, Chapman and Hall, London, 1971. |
| | Gütlich, P., Link, R. and Trautwein, A., Mössbauer Spectroscopy and Transition Metal Chemistry, Springer-Verlag, Berlin, 1978. |
| | Hawthorne, F.C. (ed.) Spectroscopic Methods in Mineralogy and Geology, Rev. Mineral. Vol. 18, Mineralogical Society of America, 1988. See Chapter on Mössbauer Spectroscopy, F.C. Hawthorne, p. 255-340. |
| | Long, G.L. and Grandjean, F. (eds.) Mössbauer Spectroscopy Applied to Inorganic Chemistry, Vols. 1-3; Mössbauer Spectroscopy Applied to Magnetism and Materials Science, Vols. 1-2, Plenum Press, New York and London, 1984, 1987, 1989, 1993, 1996. |
| | Robinson, J.W. (ed.) Handbook of Spectroscopy, Vol. 3, CRC Press, Inc., Boca Raton, USA, 1981. See Chapter on Mössbauer Spectroscopy, J.G. Stevens (ed.), p. 403-528. |
| Journal | Analytical Chemistry (American Chemical Society, Washington DC) contains biennial reviews (starting in 1966) of Mössbauer spectroscopy, see for example Vol. 62, p. 125R-139R, 1990. |
| | Hyperfine Interactions (J.C. Baltzer AG, Basel) publishes proceedings from various Mössbauer conferences, see for example Vol. 68-71, 1992. |
| | Mössbauer Effect Reference and Data Journal (Mössbauer Effect Data Center, Asheville, NC) contains references and Mössbauer data for nearly all Mössbauer papers published. |
| Data Resource | Mössbauer Effect Data Center Mössbauer Information System (maintained by the Mössbauer Effect Data Center, Asheville, NC) contains extensive bibliographic and Mössbauer data entries compiled from the Mössbauer literature. Searches of the database are possible; contact the Mössbauer Effect Data Center for details (http://www.unca.edu/medc). |
| | Stevens, J.G., Pollack, H., Zhe, L., Stevens, V.E., White, R.M. and Gibson, J.L. (eds.) Mineral: Data and Mineral: References, Mössbauer Handbook Series, Mössbauer Effect Data Center, University of North Carolina, Asheville, North Carolina, USA, 1983. |
| | Mössbauer Micro Databases (Mössbauer Effect Data Center, Asheville, NC) cover many topics including Minerals. Databases are set up to run on IBM-compatible microcomputers and can be searched using various options. |
| | Mössbauer Information Exchange (MIX) is a project of the KFKI Research Institute for Particle and Nuclear Physics, Budapest, Hungary. It includes an e-mail list, archives of programs and other documents, databases, current information and relevant links, all accessible through their world wide web site (http://www.kfki.hu/~mixhp/). |

temperature and pressure. Often phase transformations involve only small changes in the atomic environment, so in these cases it is only through observation of hyperfine parameter trends with temperature or pressure that a transformation can be identified using Mössbauer spectroscopy.

**Isomer shift**

The isomer shift arises through an electric monopole interaction between the positive nuclear charge and the electric field of the surrounding electrons. This interaction causes a shift of the nuclear energy levels compared to an unperturbed nucleus, where the magnitude of the shift is a function of the difference in *s*-electron densities between the source and absorber nuclei (Fig. 1). In addition to the intrinsic (or chemical) isomer shift, $\delta_0$, there is also a small shift due to atomic vibrations, called the second-order Doppler shift, $\delta_{SOD}$. The second-order Doppler shift is a strong function of temperature and decreases to zero at 0 K. Experimentally the total shift of the Mössbauer spectrum from the reference zero point is simply $\delta_0 + \delta_{SOD}$. To avoid confusion, the experimentally observed shift is generally referred to as the *centre shift*, and is generally given the unsubscripted symbol $\delta$. The contribution from $\delta_{SOD}$ is similar for most standard materials, so for purposes of comparison the isomer shift is often taken to be equal to the centre shift. All energy shifts are measured relative to a reference zero point, which is conventionally taken to be the centre shift of $\alpha$-Fe at room temperature and pressure.

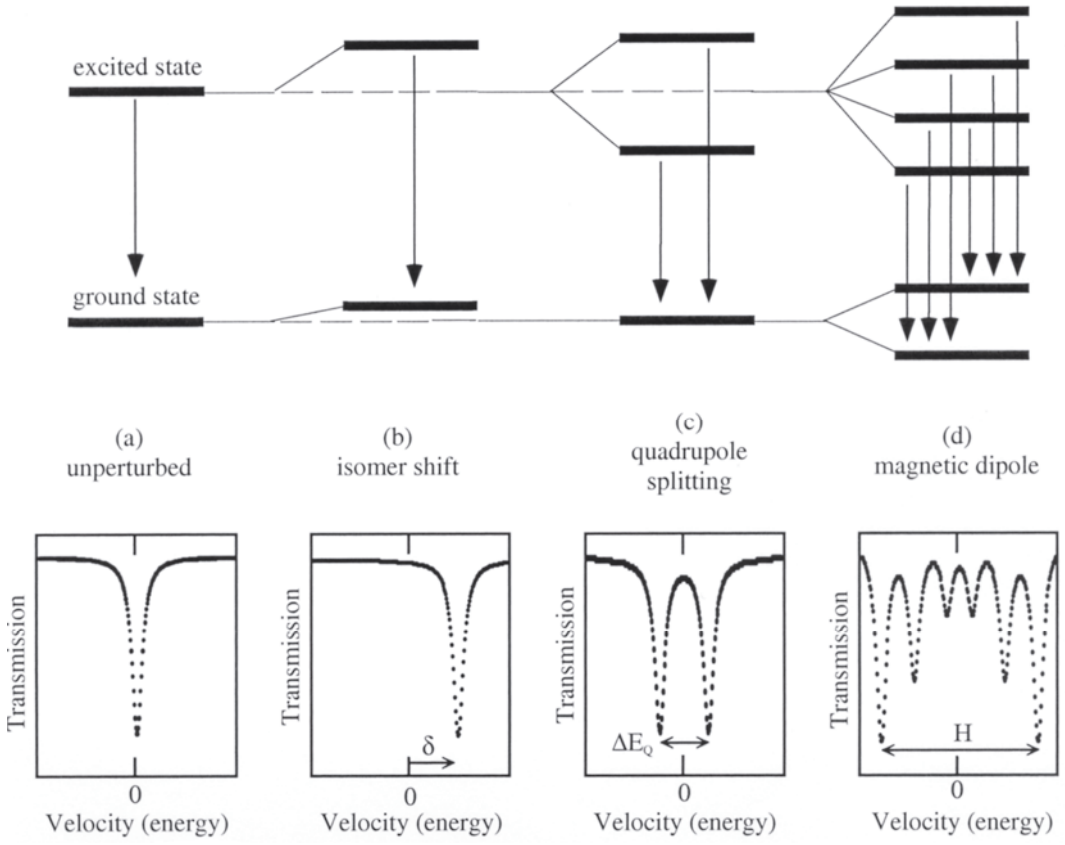


**Figure 1.** Hyperfine interactions for $^{57}$Fe nuclei, showing the nuclear energy level diagram for (a) an unperturbed nucleus; (b) electric monopole interaction (isomer shift); (c) electric quadrupole interaction (quadrupole splitting); and (d) magnetic dipole interaction (hyperfine magnetic splitting). Each interaction is shown individually, accompanied by the resulting Mössbauer spectrum.

to discriminate between different valence states, spin states and coordinations of the absorber atoms. Ideally we would like to be able to calculate the centre shift expected for a specific structural and electronic configuration, but advances in computational methods The isomer shift is related to the *s*-electron density, which is in turn affected by *p*- and *d*-electrons through shielding effects. The observed centre shift can therefore be used have not yet progressed to the point where this is possible for most minerals. Empirically it has been noted that centre shifts for different configurations of Fe fall into specific ranges (Fig. 2), and although there is some overlap, they generally serve to identify the spin state, valence state and (usually) coordination number corresponding to a given iron site.

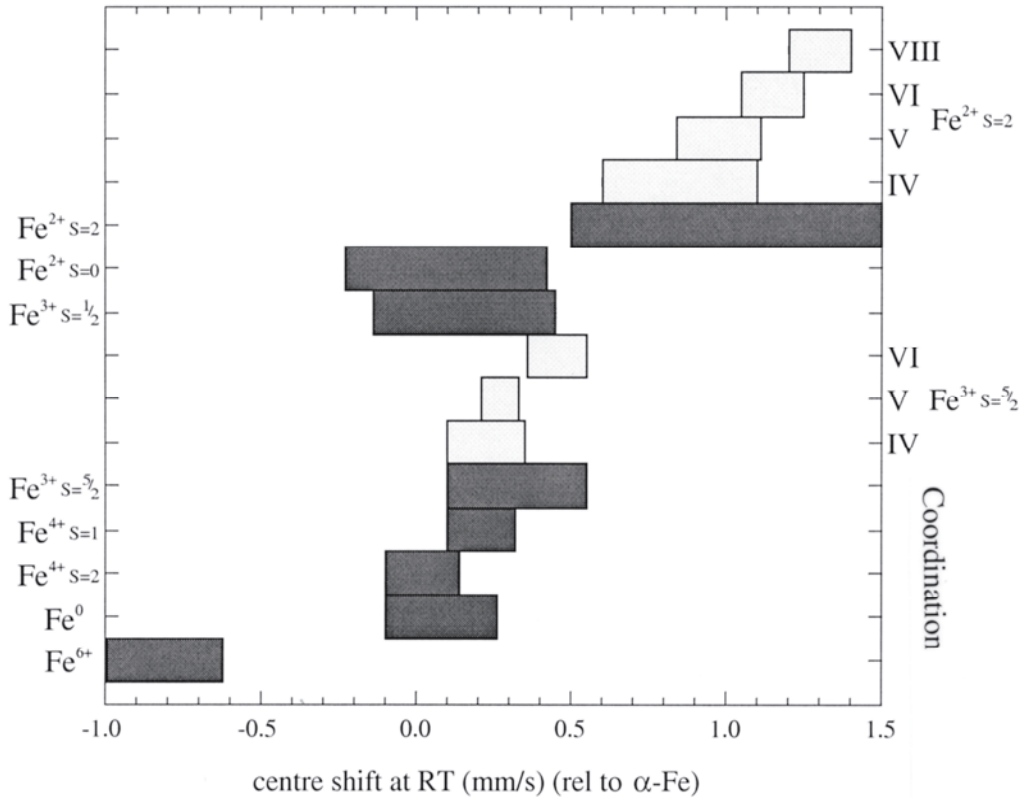


**Figure 2.** Approximate range of room temperature centre shifts (relative to α-Fe) observed for iron compounds. Black bars refer to data compiled from Greenwood and Gibb (1971), Maddock (1985) and Hawthorne (1988). Grey bars represent ranges for high-spin $Fe^{2+}$ and $Fe^{3+}$ in minerals reported by Seifert (1990), where additional data from Burns and Solberg (1990) have been added for pentacoordinated $Fe^{3+}$.

The temperature dependence of the isomer shift can be written

$$\delta(T) = \delta_0(T) + \delta_{SOD}(T). \quad (1)$$

To a first approximation, the variation of δ with temperature reflects changes in $\delta_{SOD}$ only, which can be expressed using the Debye model as

$$\delta_{SOD}(T) = -\frac{9}{16}\frac{k_B \Theta_M}{mc} - \frac{9}{2}\frac{k_B T}{mc}\left(\frac{T}{\Theta_M}\right)^3 \int_0^{\Theta_M/T} \frac{x^3 dx}{e^x - 1}, \qquad T < \Theta_M \quad (2)$$

where *m* is the mass of the Mössbauer isotope, $k_B$ is the Boltzmann constant, c is the speed of light and $\Theta_M$ is the characteristic Mössbauer temperature (Pound and Rebka 1960). $\Theta_M$ should not be confused with the Debye temperature, $\Theta_D$, determined from

specific heat measurements, which is based on a different weight of the phonon frequency distribution (e.g. Kolk 1984). The isomer shift, $\delta_0$, also has a temperature dependence through the volume effect and the change in population of the electron orbitals (e.g. Perkins and Hazony 1972), but generally this is significantly smaller than the temperature dependence of $\delta_{SOD}$. A phase transformation may be recognised from a plot of centre shift versus temperature either (1) as a discontinuity if there is significant structural rearrangement and hence a change in the value of $\delta_0(T)$; or (2) as an anomalous value of $\Theta_M$ fitted to the data if there is a more subtle or a continuous change to the atomic environment. Typical values for $\Theta_M$ are given by De Grave and Van Alboom (1991).

Both the isomer shift, $\delta_0$, and the second-order Doppler shift, $\delta_{SOD}$, are pressure dependent through the volume dependence of the electronic charge density at the nucleus. The pressure dependence of the centre shift at constant temperature can be approximated by

$$\partial\delta/\partial \mathrm{P} = \partial\delta_0/\partial \mathrm{P} + \partial\delta_{SOD}/\partial \mathrm{P}. \tag{3}$$

The volume dependence of $\delta_{SOD}$ can be estimated following the method of Williamson (1978):

$$\frac{\partial \delta_{SOD}}{\partial \ln V} = \gamma \frac{9\mathbf{k}_B\Theta_D}{16m\mathbf{c}} F\left(T/\Theta_D\right) \tag{4}$$

where $\gamma$ is the lattice Grüneisen parameter, $\Theta_D$ is the lattice Debye temperature and the other symbols are as for Equation (1). The function $F$ is given by:

$$F\left(T/\Theta_D\right) = 1 + \frac{8}{e^{\Theta_{D/T}} - 1} - 24\left(T/\Theta_D\right)^4 \int_0^{\Theta_{D/T}} \frac{x^3}{e^x - 1}\, dx. \tag{5}$$

The volume dependence of $\delta_{SOD}$ is positive, implying that $\delta_{SOD}$ decreases with increasing pressure, but increases with increasing temperature. The effect of pressure on the isomer shift is more difficult to determine, and for $^{57}$Fe compounds can be affected by (1) changes in orbital occupation; and (2) distortion of the wavefunctions—either compression of the *s* electrons or spreading out of the 3*d* electrons (increase in covalency) (Drickamer et al. 1969). The second factor, an increase in covalency, causes an increase in *s* electron density and hence a decrease in $\delta_0$. The first factor includes transfer of electrons between the iron 3*d* and 4*s* levels, between different iron 3*d* levels, and between iron orbitals and orbitals of the coordinating anions. It can either increase or decrease $\delta_0$ depending on the nature and direction of transfer. Generally the pressure effect on $\delta_0$ is significantly greater than for $\delta_{SOD}$, so the latter is often taken to be zero (Amthauer 1982), although there are exceptions (e.g. McCammon and Tennant 1996). A phase transformation may be recognised from a plot of centre shift versus pressure either (1) as a discontinuity if there is a significant change in bonding and/or crystal structure; or (2) as a change in slope if the change to the atomic environment is more subtle.

**Quadrupole splitting**

Quadrupole splitting arises through a quadrupole interaction between the nuclear quadrupolar moment and the electric field gradient (EFG) at the nucleus due to the surrounding electrons, causing a splitting of the nuclear energy states. In the case of $^{57}$Fe the excited state is split into two levels, giving rise to a doublet with equal component linewidths and areas in the ideal random absorber case (Fig. 1). For the case of an oriented absorber, the areas vary according to the angle between the principal axis of the EFG ($V_{zz}$) and the propagation direction of the $\gamma$-ray. The quadrupole splitting, $\Delta E_Q$, measures the difference in energy between the excited states, and can be expressed as

$$\Delta E_Q = \frac{1}{2} eQV_{zz}\sqrt{1+\frac{\eta^2}{3}} \tag{6}$$

where $Q$ is the nuclear quadrupole moment, e is the electron charge, $V_{zz}$ is the principal component of the EFG tensor and $\eta$ is the asymmetry parameter, where $\eta = (V_{xx} - V_{yy})/V_{zz}$ and $0 \le \eta \le 1$. According to the static crystal-field model of Ingalls (1964), the EFG components can be related to crystal and electronic structural factors through the following:

$$V_{zz} = (1-R)eq_{val} + (1-\gamma_\infty)eq_{lat}$$

$$V_{xx} - V_{yy} = (1-R)e\eta_{val}q_{val} + (1-\gamma_\infty)e\eta_{lat}q_{lat}, \tag{7}$$

where the subscript "val" refers to the asymmetric charge distribution of the valence electrons, and the subscript "lat" refers to the deviation from cubic symmetry of the neighbouring atoms in the crystalline lattice. R and $\gamma_\infty$ are the Sternheimer shielding and anti-shielding factors, respectively, and are added to correct for polarisation effects. The valence and lattice contributions can be cast in terms of a reduction function, $F$:

$$\Delta E_Q = \Delta E_{Q,val}(0)F\left(\Delta_1, \Delta_2, \lambda_0, \alpha^2, T\right) + \Delta E_{Q,lat} \tag{8}$$

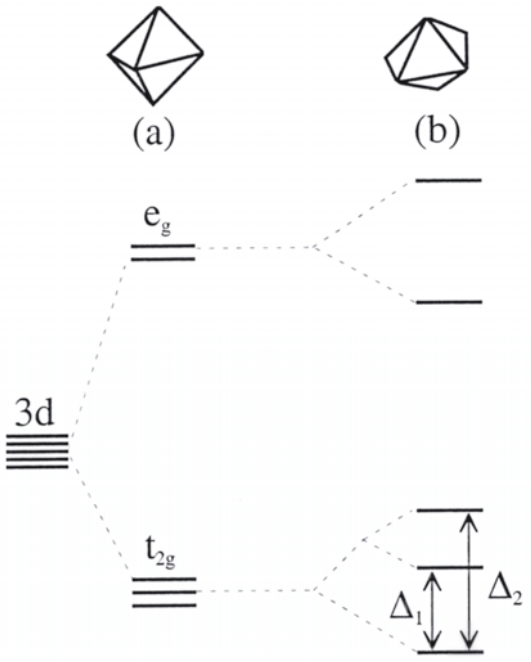


**Figure 3.** Energy levels of 3*d* electrons in (a) regular octahedron; (b) highly distorted octahedron. The splitting of energy levels in the ground state are given by $\Delta_1$ and $\Delta_2$ (adapted from Burns 1993).

where $\Delta E_{Q,val}(0)$ is the valence contribution at 0 K, $\alpha^2$ is a covalency factor, $\lambda_0$ is the spin-orbit coupling constant for the free ion, $T$ is the temperature, and $\Delta_1$ and $\Delta_2$ are the ground state splittings of the crystal field levels (Fig. 3). The valence and lattice contributions to the quadrupole splitting for $^{57}$Fe are always of opposite sign. Figure 4 illustrates the schematic variation of $\Delta E_Q$ with increasing values of the ground state splitting, which in the simplest case can be linked to the distortion of the site from cubic symmetry. At low distortions the lattice contribution is small, so $\Delta E_Q$ increases with increasing distortion, but at high degrees of distortion the lattice term dominates, and $\Delta E_Q$ remains constant or even decreases with increasing distortion.

The quadrupole splitting depends on the valence and spin state of the absorber atoms, as well as the coordination and degree of distortion of the crystallographic site. Values of $\Delta E_Q$ extend from zero to a maximum of approximately 3.7 mm/s for $^{57}$Fe compounds, but are less diagnostic of valence and coordination compared to the centre shift. The quadrupole splitting is more sensitive to small changes in the atomic environment, however, and there are many instances where phase transformations cause a change in the quadrupole splitting, but none in the centre shift.

The quadrupole splitting is sensitive to temperature primarily through the valence contribution, which reflects the temperature dependence of electrons between different

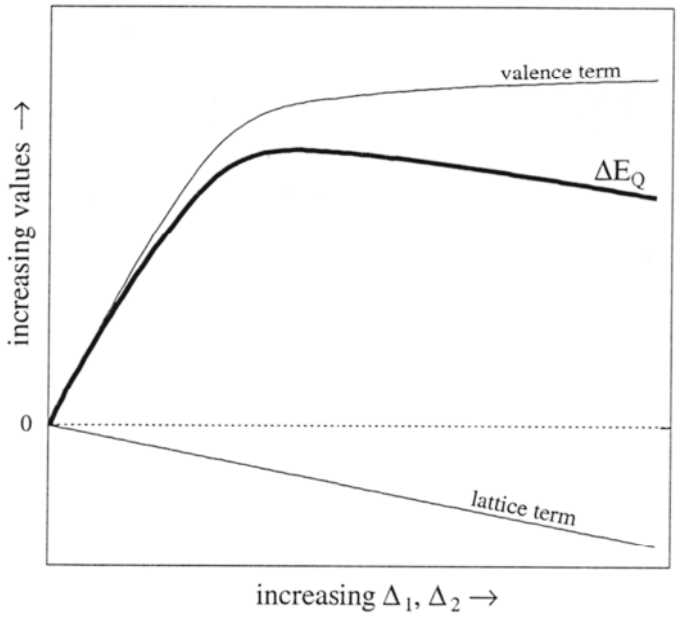


**Figure 4.** Schematic variation of the valence and lattice term contributions to the quadrupole splitting with increasing values of the 3*d* ground state splittings, $\Delta_1$ and $\Delta_2$. The quadrupole splitting, $\Delta E_Q$, is the sum of the valence and lattice terms (adapted from Ingalls 1964).

energy levels. The lattice term is sensitive to temperature only through changes in the relative position of neighbouring atoms, and such changes are generally negligible unless a phase transformation takes place. The crystal field model of Ingalls (1964) can be used to fit experimental quadrupole splitting data as a function of temperature in order to extract parameters such as the ground-state splittings, and these can be useful for comparison on both sides of a phase transformation to provide an insight into changes to electronic structure through the transformation.

The quadrupole splitting is sensitive to pressure through both the valence and lattice terms as well as the covalency effect, and may increase or decrease with pressure, depending on the relative magnitude of these contributions. Similar to the temperature variation, the pressure variation of the quadrupole splitting is more likely than the centre shift to show either a discontinuity or a change in slope when a phase transformation occurs.

## Hyperfine magnetic splitting

Magnetic splitting arises through a dipole interaction between the nuclear magnetic dipole moment and a hyperfine magnetic field at the nucleus, causing a splitting of the nuclear energy states. In the case of $^{57}$Fe the excited state is split into four levels and the ground state into two levels, giving eight possible transitions. In the absence of a quadrupole interaction, the selection rules for magnetic dipole interactions allow only six transitions to occur, which in the ideal random absorber case give a sextet with equal component linewidths and relative line areas in the ratio 3:2:1:1:2:3 (Fig. 1). For the case of an oriented absorber, the areas vary according to the angle between the hyperfine field direction and the propagation direction of the γ-ray. In the absence of a strong quadrupole interaction, the energy difference between the outer two lines is proportional to the magnitude of the hyperfine magnetic field.

The hyperfine magnetic field seen at the nucleus can be written as the vector sum of three components:

$$\mathbf{H} = \mathbf{H}_c + \mathbf{H}_{dip} + \mathbf{H}_{orb}. \quad (9)$$

The first term, $\mathbf{H}_c$, generally has the largest magnitude, and is related to the spin density at the nucleus (Fermi contact term). $\mathbf{H}_{dip}$ and $\mathbf{H}_{orb}$ arise from the dipolar interaction of the magnetic moment of the atom with the nucleus (dipolar term), and the orbital angular momentum of the atom (orbital term), respectively. The relative size of each term determines the sign and magnitude of the internal field, where the orbital and dipolar terms have opposite signs to the Fermi contact term. In the case of $^{57}$Fe, magnetically-ordered compounds containing high-spin $Fe^{3+}$ tend to have large negative hyperfine magnetic fields due to the large value of the Fermi contact term, while magnetically-ordered high-spin $Fe^{2+}$ compounds tend to have smaller fields which may be positive or negative, depending on the values of the competing orbital and dipolar fields.

Hyperfine magnetic splitting is seen in a Mössbauer spectrum when the hyperfine magnetic field is present at the nucleus over a period longer than the Larmor precession time. In the case of paramagnetic absorbers, spin-spin and spin-lattice relaxation times are generally much faster than the Larmor precession time, hence the average field seen at the nucleus is zero and no magnetic splitting is observed. Below the Curie or Néel temperature, however, magnetic exchange interactions establish a hyperfine magnetic field on a significantly longer timescale, hence magnetic splitting is observed. If the timescale of magnetic fluctuations is comparable to the Larmor precession time, relaxation effects cause broadening and changes to the lineshape of the resulting Mössbauer spectrum.

The variation of the magnetic hyperfine field with temperature provides information on the bulk magnetic properties. For absorbers where **H** is dominated by the Fermi contact term (e.g. high-spin $Fe^{3+}$ compounds), the hyperfine magnetic field measured by Mössbauer spectroscopy is proportional to the sublattice magnetisation, and the simplest model that describes the variation of magnetisation with temperature is the Weiss molecular field theory (originally described by Weiss 1906). Using this model the temperature dependence of the hyperfine magnetic field is given by the equation

$$H(T) = H_0 B_J\left(\frac{3J}{(J+1)}\frac{H(T)}{H_o}\frac{T_m}{T}\right) \quad (10)$$

(see Morrish 1965 for a derivation) where $H_0$ is the saturation field at $T = 0$ K, $T_m$ is the magnetic transition temperature, $J$ is the total angular momentum, and the Brillouin function $B_J(x)$ is defined as

$$B_J(x) = \frac{2J+1}{2J}\coth\left[\frac{2J+1}{2J}x\right] - \frac{1}{2J}\coth\left(\frac{x}{2J}\right). \quad (11)$$

$T_m$ represents the temperature at which the thermal energy becomes equal to the magnetic exchange energy, and is related to the strength of exchange interactions between atomic dipoles. In the case where there are substantial contributions to the hyperfine magnetic field from $\mathbf{H}_{orb}$ and $\mathbf{H}_{dip}$ (e.g. high-spin $Fe^{2+}$ compounds), the hyperfine magnetic field may not be strictly proportional to the magnetisation, and hence $T_m$ in Equation (10) might not reflect the bulk magnetic transition temperature. In this case, however, it is possible to determine the latter quantity from relative line intensities of spectra collected under applied magnetic fields (e.g. Johnson 1989). The value of $|\mathbf{H}|$ is likely to change at

phase transformations that involve structural rearrangement, but may also change at magnetic transitions such as a spin reorientation. In the case where changes to |**H**| are more subtle, a plot of hyperfine field versus temperature fitted to Equation (10) may indicate the transition temperature.

The hyperfine magnetic field is sensitive to pressure mainly through the value of the Fermi contact term, and can be affected by the competing effects of enhanced spin density due to reduced interatomic distances, or decreased spin density due to changes in interatomic angles that reduce magnetic exchange interactions. A phase transformation may be recognised from a plot of hyperfine field versus pressure either as a discontinuity or a change in slope.

**Table 2.** Appearance of magnetic hyperfine Mössbauer spectra with ideal sextet intensity ratios for various magnetic structures as a function of applied magnetic field.

| *External field* | *Ferromagnet* | *Antiferromagnet* | *Ferrimagnet* | *Canted antiferromagnet* |
|---|---|---|---|---|
| | ↑↑↑↑ | ↑↓↑↓ | ↑↓↑↓ | ↖↖↗↗ |
| $\mathbf{H}_{ext} = 0$ | one subspectrum | one subspectrum | two subspectra | one subspectrum |
| $\mathbf{H}_{ext}$ // easy axis | one subspectrum<br>$\mathbf{H}_{obs} = \mathbf{H}_{hf} + \mathbf{H}_{ext}$<br>3:0:1:1:0:3 | two subspectra<br>$\mathbf{H}_{obs} = \mathbf{H}_{hf} \pm \mathbf{H}_{ext}$<br>3:0:1:1:0:3 | two subspectra<br>$\mathbf{H}_{obs} = \mathbf{H}_{hf} \pm \mathbf{H}_{ext}$<br>3:0:1:1:0:3 | one subspectrum<br>$\mathbf{H}_{obs} = \mathbf{H}_{hf} + \mathbf{H}_{ext}$<br>3:*x*:1:1:*x*:3 |

In addition to variations in temperature and pressure, application of an external magnetic field can also induce phase transformations. These involve changes to the magnetic structure of an ordered array of atomic spins that is described by the relative alignment of spins to each other, and the orientation of the spins to the crystallographic axes. Mössbauer spectroscopy can be used to deduce the arrangement of atomic spins through one or more of the following: (1) spectral fitting to determine the number of magnetic subspectra compared to the number of iron sites in the crystal lattice; (2) application of an external magnetic field to determine the effect on the resulting hyperfine field; and (3) application of an external magnetic field to determine the change in the relative areas of component lines in the magnetic subspectra (Table 2). Similar methods can be used to deduce changes to the magnetic structure under the influence of an externally applied magnetic field.

## Relative area

The area of the absorption line is related to the number of iron atoms per unit area of the absorber. The expression is complex in most cases, however, so Mössbauer spectroscopy is generally not a practical method for determining absolute iron concentrations. The situation is more favourable, however, for determination of relative abundances based on relative spectral areas. For this discussion it is useful to define the dimensionless absorber thickness

$$t_a = \sigma_0 f_a n_a \tag{12}$$

where $\sigma_0$ is the cross-section at resonance for the Mössbauer transition (= $2.56 \times 10^{-18}$ cm$^2$ for $^{57}$Fe), $f_a$ is the recoil-free fraction of the absorber, and $n_a$ is the number of $^{57}$Fe atoms per cm$^2$. A corresponding dimensionless thickness can be defined for the source. In the thin source and absorber approximation ($t_a$, $t_s << 1$), the total spectral area can be written as the sum of the individual subspectral contributions, where the area of each subspectrum is proportional to the total number of $^{57}$Fe atoms occupying the corresponding site. The thin source approximation is usually satisfied for conventional $^{57}$Co sources (but not point sources!), while the thin absorber approximation as given above usually is not. The extent to which the condition $t_a << 1$ can be relaxed in the case of intrinsically broadened linewidths (arising from differences in next-nearest neighbour configurations, for example) is discussed by Ping and Rancourt (1992).

In the thin source and absorber approximation, the area of the subspectrum corresponding to the *i*th site can be written

$$A_i \propto f_s t_{a,i} \Gamma_i = \sigma_0 f_s \Gamma_i f_{a,i} n_{a,i} \tag{13}$$

where $\Gamma_i$ is the linewidth, which according to Margulies and Ehrmann (1961) can be represented for absorber thicknesses up to $t_a \approx 4$ by

$$\Gamma_i = \Gamma_0 (2 + 0.27 t_a), \tag{14}$$

where $\Gamma_0$ is the natural linewidth (= 0.097 mm/s for $^{57}$Fe). In the case of non-overlapping lines, the relative areas can be used through the above equations to determine the relative abundance of the Mössbauer nuclei in the sites corresponding to the different subspectra. Equation (13) is not valid when the thin absorber approximation is not fulfilled, however. Calculations by Rancourt (1989) illustrate the extent to which relative area fractions are overestimated with increasing absorber thickness, and a subsequent paper by Rancourt et al. (1993) provides guidelines for calculating absorber thicknesses where the thin absorber approximation is still approximately valid.

The relative area of the Mössbauer spectrum depends on temperature primarily through changes in the recoil-free fraction of the absorber (Eqn. 13). The variation of $f_a$ with temperature can be determined from the Debye model

$$f(T) = exp\left\{ -\frac{3}{2} \frac{E_R}{k_B \Theta_M} \left[ 1 + 4 \left( \frac{T}{\Theta_M} \right)^2 \int_0^{\Theta_M/T} \frac{x dx}{e^x - 1} \right] \right\} \tag{15}$$

(Mössbauer and Wiedemann 1960) where $E_R$ is the recoil energy (= 3.13425 x $10^{-22}$ J for the 14.4 keV transition of $^{57}$Fe), $k_B$ is the Boltzmann constant, and $\Theta_M$ is the characteristic Mössbauer temperature, where $\Theta_M$ can be determined from temperature dependant measurements of the centre shift as described by Equation (2). The recoil-free fraction of the absorber can also be determined through temperature dependant measurements of the relative area according to Equation (13). In either case, a phase transformation can be recognised as either a discontinuity or a change in slope of the recoil-free fraction plotted as a function of temperature.

The relative area of the Mössbauer spectrum varies with pressure also primarily through changes in the recoil-free fraction of the absorber (Eqn. 13). The volume dependence of the recoil-free fraction is similar to that of $\delta_{SOD}$, since both are related to the value of $\Theta_M$ (Eqns. 2 and 15). The recoil free fraction therefore increases with pressure, and similar to the temperature variation discussed above, a phase transformation could cause either a discontinuity or a change in slope in the variation of recoil-free fraction with pressure.

## INSTRUMENTATION

A Mössbauer apparatus is relatively simple and can be divided into three parts – the source, the absorber and the detector. The modular nature of the spectrometer enables Mössbauer spectroscopy to be performed under varying conditions in a number of different configurations. Many of these can be interchanged and are listed in Figure 5.

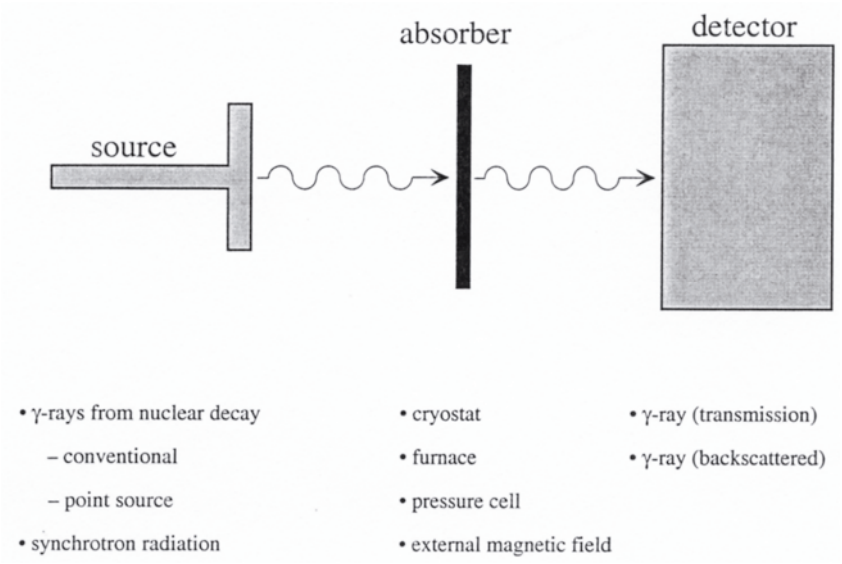


**Figure 5.** Schematic view of a Mössbauer spectrometer showing various possibilities for the source, absorber and detector. Nearly all the individual configurations are independent, enabling numerous combinations to be made.

Variables that can be applied to the absorber include temperature, pressure and magnetic field. The absorber can be placed inside a cryostat (e.g. Williams 1975) or a furnace (e.g. Kolk et al. 1985), or it can be placed inside a pressure device such as a diamond anvil cell (DAC) (e.g. Pasternak and Taylor 1996). Simultaneous $P$,$T$ measurements can be made through combination of the above, such as a DAC + cryostat (Hearne et al. 1994) and a DAC + furnace (Hålenius et al. 1996). External magnetic fields can be applied to the absorber (e.g. Craig 1965) and combined with studies under high pressure and variable temperature.

The source is generally a radioactive parent of the Mössbauer isotope, and γ-rays are produced through nuclear decay. For radioactive parents that are magnetically ordered, such as $^{57}$Co, a non-magnetic matrix is used (e.g. Rh) to dilute the atoms sufficiently such that the emitted radiation is a single energy with no detectable broadening by magnetic interactions and a low probability of self-absorption (i.e. absorption by another nucleus in the source). The latter ensures that the source thickness (which affects the linewidth and recoil-free fraction) does not increase significantly with time. The source diameter is then determined by the number of parent nuclei required to achieve a sufficient count rate, and for conventional $^{57}$Co sources is of the order 1 cm. This diameter can be significantly reduced if the density of parent nuclei is increased to the level where broadening due to magnetic interactions just starts to occur. For $^{57}$Co nuclei, this enables the source to be reduced to a diameter of ca. 500 μm without significant loss in count rate. The penalty, however, is a rapid increase in source thickness, which limits the useable lifetime of the source. Such concentrated sources, so-called "point sources", are essential for high-

pressure experiments, but can also be used to record Mössbauer spectra of microscopic samples ($d \geq 50$ μm) at ambient conditions (McCammon et al. 1991, McCammon 1994).

Source radiation can also be generated by a particle accelerator, such as a synchrotron facility. There are many advantages to such an experiment, including the possibility for a small beam size with high signal/noise ratio that does not suffer from the limitations described above. Some recent reviews are given by Arthur (1996) and Ruffer and Chumakov (1996).

The geometry of the Mössbauer spectrometer can be varied depending on the type of experiment. Transmission studies require a linear arrangement where the detector sits behind the source and absorber, such as illustrated in Figure 5, and provide information on all $^{57}$Fe nuclei in the absorber. The detector can also be placed in a backscattering geometry between the source and absorber, enabling the study of only the surface nuclei in the absorber. Recent reviews of the latter technique, called Conversion Electron Mössbauer Spectroscopy (CEMS) are given by Nomura et al. (1996) and Gancedo et al. (1997).

Many of the above possibilities for source, absorber and detector can be combined, enabling a wide range of instrumental possibilities to use Mössbauer spectroscopy in the study of phase transformations. Additional possibilities are provided through absorber and source preparation for Mössbauer isotopes such as $^{57}$Fe that have a high absorption cross section. For example, $^{57}$Fe has a natural abundance of only 2.14%, yet adequate signal/noise ratios can be obtained for absorbers containing as little as 5 wt % FeO. This enables enriched $^{57}$Fe to be used for preparation of synthetic samples with barely detectable amounts of Fe; hence phase transformations can be studied in nearly iron-free systems. $^{57}$Fe can be added homogeneously to study bulk properties, or it can be added inhomogeneously (e.g. deposited in a thin layer) to study surface properties. The same enrichment possibilities exist for $^{57}$Co as a source (in this case a single-line absorber would be used), although experimentally it is more difficult due to the need to work with radioactive materials.

Collection of $^{57}$Fe Mössbauer spectra with adequate signal/noise ratios requires a minimum of several hours under ideal conditions, extending to several days or weeks for experiments where conditions are less than optimal. This is most relevant for *in situ* experiments, because it limits the number of temperatures and/or pressures at which spectra can be collected. One technique that avoids this limitation is thermal scanning (e.g. Nolle et al. 1983), although the information provided is generally limited to only the phase transformation temperature.

## APPLICATIONS

Since its discovery in 1958, the Mössbauer effect has been used to characterise the nature of numerous phase transformations. As of 1999, the Mössbauer Effect Data Center has reported nearly 5000 papers that were published with keywords relating to phase transformations. The sensitivity of the Mössbauer effect enables its use not only for detecting phase transformations, but through the hyperfine parameters and their variation with temperature, pressure and magnetic field, allows a detailed characterisation of the nature of the phase transformation. The following provides a brief survey of applications of Mössbauer spectroscopy for studying different types of phase transformations. It is not intended to be a comprehensive review, but rather provides a sense of the current state of the art. A number of reviews have appeared on the application of Mössbauer

spectroscopy to phase transformations that can be consulted for further information (Shenoy 1973, Wertheim 1973, Preston 1978, Johnson 1989, Seifert 1990).

## Structural transformations

***Structure modification.*** Phase transformations that involve a change in coordination number of the site containing the Mössbauer nucleus generally involve large changes to the hyperfine parameters, while those that involve modification only in the second coordination shell may show smaller changes. The quadrupole splitting and hyperfine magnetic field (if present) are generally the most sensitive to such changes. This is illustrated by pressure-induced phase transformations in the compound $Fe_xMg_{1-x}SiO_3$, which for values of $x \approx 0.1$ include the following structures:

orthopyroxene → clinopyroxene → garnet → perovskite

(e.g. Akaogi et al. 1992, Woodland and Angel 1997). The transformation from orthopyroxene to clinopyroxene involves changes primarily in the second coordination shell, and cannot be quenched to ambient conditions. McCammon and Tennant (1996) studied the transition in $FeSiO_3$ *in situ* as a function of pressure at room temperature, and were able to identify the phase transformation from a discontinuity in the quadrupole splitting variation with pressure, while the centre shift data showed (at most) a break in slope. From the relative changes to the hyperfine parameters, they were able to extract information regarding the electronic structure and site distortion that could be correlated with high-pressure data from optical spectroscopy and X-ray diffraction. The phase transformation of $Fe_xMg_{1-x}SiO_3$ from the pyroxene to the garnet and perovskite structures involves a change to the coordination number of the iron sites, and both can be quenched to ambient conditions. Table 3 lists the hyperfine parameters of all polymorphs at room temperature, and illustrates (1) the minimal change to hyperfine parameters between the orthopyroxene and clinopyroxene structures, the largest being the quadrupole splitting of the M1 site which was used by McCammon and Tennant (1996) to identify the phase transformation at high pressure; (2) the slightly larger change to the centre shift of $Fe^{2+}$ between six-fold and eight-fold coordination compared to the negligible change between six-fold and the 8-12 coordinated site of the perovskite structure, the latter due to factors including site distortion and reduced $Fe^{2+}$-O distance; and (3) the large difference in quadrupole splitting of $Fe^{2+}$ for sites with the same coordination number, due primarily to differences in distortion between the sites.

**Table 3.** Room temperature hyperfine parameters for $Mg_{1-x}Fe_xSiO_3$ polymorphs.

| *Structure* | $x_{Fe}$ | *Site* | $\delta$ *(mm/s)* | $\Delta E_Q$ *(mm/s)* | *Reference* |
|---|---|---|---|---|---|
| **opx** | 0.1 | $^{VI}Fe^{2+}$ M1 | 1.171(5) | 2.49(1) | [1] |
| | | $^{VI}Fe^{2+}$ M2 | 1.142(5) | 2.11(1) | |
| **cpx** | 0.11 | $^{VI}Fe^{2+}$ M1 | 1.175(5) | 2.58(1) | [1] |
| | | $^{VI}Fe^{2+}$ M2 | 1.139(5) | 2.11(1) | |
| **garnet** | 0.1 | $^{VI}Fe^{2+}$ | 1.146(5) | 1.26(1) | [1] |
| | | $^{VIII}Fe^{2+}$ | 1.259(5) | 3.60(1) | |
| **perovskite** | 0.09 | $^{VIII\text{-}XII}Fe^{2+}$ | 1.13(1) | 1.77(2) | [2] |

References: [1] McCammon, unpublished data; [2] Lauterbach et al. (2000)

***Order-disorder.*** Phase transformations that involve the long-range ordering of cations over two or more lattice sites can generally be studied using Mössbauer spectroscopy if one of the atoms has a Mössbauer transition, and the resulting spectrum is sufficiently resolved that robust relative areas can be determined. One classic example is the pyroxene solid solution $MgSiO_3$-$FeSiO_3$, which has been studied in both the ortho- (e.g. Virgo and Hafner 1969, Skogby et al. 1992, Domeneghetti and Stefan 1992) and clino- (Woodland et al. 1997) structure modifications. Careful analysis of the relative areas enabled site occupancies to be extracted that were consistent with structure refinements, and allowed a long-range order parameter to be calculated. Short-range ordering of isovalent cations involving the Mössbauer atom is more difficult to study, since one is looking for differences in next-nearest neighbour configurations. These generally cause slight variations in hyperfine parameters that give rise to broadened, asymmetrical spectral lines. Spectra can be analysed and compared with results expected from possible arrangements, and in some cases it is possible to deduce whether atoms are randomly distributed or arranged in clusters, such as in the system $FeCr_2S_4$-$FeRh_2S_4$ thiospinel (Riedel and Karl 1980) and $MgSiO_3$-$FeSiO_3$ clinopyroxene (Angel et al. 1998). A similar situation exists for ordering studies that involve non-Mössbauer isovalent cations, since effects also occur only in the next-nearest neighbour shell. In these cases, however, it is generally not even possible to distinguish between short- and long-range ordering from the Mössbauer data, since the hyperfine parameters are only affected by, at most, the second coordination shell.

Ordering of anions or lattice defects (which for the purposes of this discussion include heterovalent cation and anion substitutions) generally involve greater changes to the environment of the Mössbauer nucleus, and hence to the hyperfine parameters. A classic example is wüstite, $Fe_xO$, where broad quadrupole splitting distributions in the spectra can be interpreted in terms of the most likely defect cluster arrangements (e.g. Greenwood and Howe 1972, McCammon and Price 1985). Broadening of Mössbauer spectra has been interpreted to indicate short-range ordering of heterovalent cations in aluminous orthopyroxene (Seifert 1983). A different approach can be taken if additional information is available, such as from structure or composition. McCammon et al. (2000) were able to deduce short-range ordering of oxygen vacancies in the system $CaTiO_3$-$CaFeO_{2.5}$ from comparison of octahedral, pentacoordinated and tetrahedral $Fe^{3+}$ site occupancies with composition data.

***Glass transitions.*** Phase transformations that involve a transition between a glass and a supercooled liquid state generally modify the recoil-free fraction at the transition, and may be accompanied by changes in quadrupole splitting and linewidth. An early review by Ruby (1973) discusses the nature of glass transitions and their observation by Mössbauer spectroscopy. One example is a high temperature study by Bharati et al. (1983) of alkali borate, alkali borosilicate and vanadate glasses containing $^{57}Fe$, where distinct softening of the lattice at the glass transition temperature is observed. Changes in the degree of polymerisation and coordination of Fe in glass can also be studied using Mössbauer spectroscopy, where *in situ* measurements are preferable to studies of quenched melts. One can combine the latter with *in situ* measurements using complementary techniques, however, such as in experiments by Wang et al. (1993) who used high temperature Raman spectroscopy to study changes to polymerisation with temperature, and then used Mössbauer spectra from quenched melts to obtain information on coordination.

Pressure-induced amorphisation studies using Mössbauer spectroscopy have been briefly reviewed by Pasternak and Taylor (1996). One example is the amorphisation of $Fe_2SiO_4$ above 40 GPa at room temperature where antiferromagnetic ordering appears to

be preserved in the glassy state (Kruger et al. 1992). This behaviour is quite different to magnetic glasses produced by rapid quenching from the melt, where magnetic order is either absent or significantly inhibited due to the loss of structural order.

**Electronic transitions**

Transitions that involve a change in electronic structure of the Mössbauer atom can generally be detected using Mössbauer spectroscopy, regardless of whether changes in atomic positions are involved or not. The isomer shift is particularly sensitive to the spin state of the iron atom (Fig. 2) and is one of the primary diagnostic tools for distinguishing spin transitions. Recent examples include $CaFeO_3$, which has been inferred to undergo a first-order transition from the high-spin ($Fe^{4+}$: $S = 2$) to the low-spin ($Fe^{4+}$: $S = 1$) state near 30 GPa from a combined *in situ* Mössbauer and X-ray diffraction study (Takano et al. 1991). The change in isomer shift at the transition point was greater than 0.2 mm/s.

Changes in isomer shift can also indicate variations in valence state, including time-dependent fluctuations. In these cases there is generally no observed change in crystal structure. For example, a fraction of $Fe^{2+}$ and $Fe^{3+}$ atoms in $(Mg,Fe)SiO_3$ perovskite are involved in electron transfer that occurs faster than the mean lifetime of the excited state ($\approx 10^{-7}$ s for $^{57}Fe$), giving rise to a subspectrum with isomer shift intermediate between $Fe^{2+}$ and $Fe^{3+}$. The process is thermally activated, as shown by temperature dependant measurements of Fei et al. (1994), who showed that the relative area of the quadrupole doublet assigned to the average valence state increases dramatically with increasing temperature. Isomer shift data combined with the observed collapse of two subspectra (corresponding to $Fe^{3+}$ and $Fe^{5+}$) into a single spectrum (corresponding to $Fe^{4+}$) have been used to infer a second-order transition in $CaFeO_3$ with increasing temperature involving the delocalisation of one of the *d* electrons (Takano et al. 1977, Takano et al. 1991).

Mössbauer spectroscopy generally cannot provide independent evidence for insulator-metal transitions, but combined with other measurements such as electrical conductivity, Mössbauer data can provide important data to elucidate aspects such as transition mechanisms. Recent electrical resistance measurements of $\alpha$-$Fe_2O_3$ show a large drop in resistivity above 50 GPa, and combined with *in situ* high-pressure Mössbauer measurements that show a loss of magnetic order at the transition, was interpreted by Pasternak et al. (1999) to indicate a Mott transition resulting from the breakdown of *d-d* electron correlations. In contrast, Rozenberg et al. (1999) found an insulator-metal transition in the perovskite $Sr_3Fe_2O_7$ above 20 GPa using electrical measurements where magnetic moments, as measured by Mössbauer spectroscopy, were preserved through the phase transition. This behaviour was interpreted to indicate band closure due to *p-p* gap closure that does not involve the *d* electrons.

**Magnetic transitions**

Transitions that involve a change to the magnetic structure of an ordered array of atomic spins can sometimes be detected by Mössbauer spectroscopy, depending on the nature of the transition. The largest effect is seen in transitions between the magnetically-ordered and non-ordered state (Curie or Néel point), providing that the magnetically-ordered state exists over a sufficient timescale (see section above). In these cases the change between a singlet or quadrupole doublet and a magnetically-split spectrum are usually unambiguous, enabling such studies to be conducted under marginal signal:noise conditions such as at very high pressures. $Fe_xO$ is paramagnetic at ambient conditions, but transforms to the antiferromagnetic phase above 5 GPa according to *in situ* Mössbauer measurements of Zou et al. (1980). However at significantly higher pressures (> 90 GPa), it transforms to a non-magnetic phase, inferred by Pasternak et al. (1997) to be diamagnetic.

Transitions involving only a change in the relative alignment of spins can be detected using Mössbauer spectroscopy, although oriented measurements are usually necessary to determine the spin direction. A classic example is the Morin transition in hematite, $\alpha$-$Fe_2O_3$, which involves a transition from a collinear antiferromagnet with spin direction along the *c* axis, to a canted structure (weak ferromagnet) with spins oriented in the basal plane. There is a change in quadrupole splitting as well as a discontinuity in the variation of hyperfine magnetic field with temperature and pressure at the Morin transition, which allowed Bruzzone and Ingalls (1983) to extract information regarding the location of atoms within the unit cell that compared well with results from high-pressure X-ray diffraction. Mössbauer measurements of oriented single crystals of the rare earth orthoferrite $TbFeO_3$ were made by Nikolov et al. (1996) at 4.2 K as a function of externally applied magnetic field. From the change in relative area of the magnetic sextet components, they were able to characterise the direction and nature of spin-reorientation transitions.

## CONCLUDING REMARKS

This chapter has presented a review of the parameters involved in Mössbauer spectroscopy within the context of phase transformations. Although the Mössbauer effect can be considered a "mature" technique, now more than forty years old, technical developments continue to expand the experimental possibilities. Spatial resolution has improved within the last decade. The development of the Mössbauer milliprobe, for example, has enabled spatial resolution to be increased by more than two orders of magnitude (McCammon et al. 1991, McCammon 1994). Further improvement of spatial resolution may be anticipated with advances in nuclear forward scattering. Other possibilities on the horizon include development of a Mössbauer electron microscope which would focus conversion electrons using conventional electron optics (Rancourt and Klingelhöfer 1994).

One aspect of Mössbauer spectroscopy that has not been widely exploited in phase transformation studies is time resolution. Studies with conventional techniques are possible over a wide range of time scales, starting from the intrinsic time scale of the $^{57}$Fe Mössbauer effect ($t \approx 10^{-8}$ s) to investigate processes such as electron transfer, to time scales of $t \approx 10^{-6}$ s to measure diffusion, to longer timescales of $t \geq 10^{3}$ s to study phase transitions, oxidation and other chemical reactions.

The range of *P*,*T* conditions over which Mössbauer spectroscopy can be performed continues to expand. Existing equipment already allows experiments to be performed to 120 GPa, but there are no obvious theoretical limitations that restrict advances to higher pressures. Experiments at high temperatures are ultimately limited by lattice vibrations, but since Debye temperatures generally increase with pressure, technical advances could increase temperature limits beyond 1200°C at high pressure, raising the intriguing possibility of *in situ* Mössbauer measurements at *P*,*T* conditions approaching those of the Earth's mantle.

## REFERENCES

Akaogi M, Kusaba K, Susaki J, Yagi T, Matsui M, Kikegawa T, Yusa H, Ito E (1992) High-pressure high-temperature stability of $\alpha PbO_2$-type $TiO_2$ and $MgSiO_3$ majorite: Calorimetric and *in situ* X-ray diffraction studies. *In* Y Syono, MH Manghnani (eds) High Pressure Research: Application to Earth and Planetary Sciences. Terra Scientific Publ Co/Am Geophys Union, Tokyo/Washington DC, p 447-455

Amthauer G (1982) High pressure $^{57}$Fe Mössbauer studies on minerals. *In* W Schreyer (ed) High-Pressure Researches in Geoscience. E. Schweizerbart'sche Verlagsbuchhandlung, Stuttgart, p 269-292

Angel RJ, McCammon CA, Woodland AB (1998) Structure, ordering and cation interactions in Ca-free $P2_1/c$ clinopyroxenes. Phys Chem Minerals 25:249-258

Arthur J (1996) How to do resonant nuclear experiments with synchrotron radiation. Il Nuovo Cimento Soc Ital Fis 18D:213-220

Bharati S, Pathasarathy R, Rao KJ, Rao CNR (1983) Mössbauer studies of inorganic glasses through their glass transition temperatures. Sol State Comm 46:457-460

Bruzzone CL, Ingalls RL (1983) Mössbauer-effect study of the Morin transition and atomic positions in hematite under pressure. Phys Rev B 28:2430-2440

Burns RG (1993) Mineralogical Applications of Crystal Field Theory, 2nd ed. Cambridge University Press, Cambridge, UK

Burns RG, Solberg TC (1990) $^{57}$Fe-bearing oxide, silicate, and aluminosilicate minerals. *In* LM Coyne, SWS McKeever, DF Blake (eds) Spectroscopic Characterization of Minerals and their Surfaces, Vol 415. American Chemical Society, Washington DC, p 262-283

Craig JR (1965) Superconducting magnets: Applications to the Mössbauer effect. *In* IJ Gruverman (ed) Mössbauer Effect Methodology, Vol. 1. Plenum Press, New York, p 135-145

De Grave E, Van Alboom A (1991) Evaluation of ferrous and ferric Mössbauer fractions. Phys Chem Min 18:337-342

Domeneghetti MC, Steffen G (1992) M1, M2 site populations and distortion parameters in synthetic Mg-Fe orthopyroxenes from Mössbauer spectra and X-Ray structure refinements. Phys Chem Min 19:298-306

Drickamer HG, Vaughn RW, Champion AR (1969) High-pressure Mössbauer resonance studies with iron-57. Accounts Chem Res 2:40-47

Fei Y, Virgo D, Mysen BO, Wang Y, Mao HK (1994) Temperature dependent electron delocalization in $(Mg,Fe)SiO_3$ perovskite. Am Mineral 79:826-837

Gancedo JR, Davalos JZ, Gracia M, Marco-Sanz JF (1997) The use of Mössbauer spectroscopy in surface studies. A methodological survey. Hyper Inter 110:41-50

Greenwood NN, Gibb TD (1971) Mössbauer Spectroscopy. Chapman and Hall, London

Greenwood NN, Howe AT (1972) Mössbauer studies of Fe(1-x)O. Part I. The defect structure of quenched samples. J Chem Soc Dalton Trans:110-116

Hålenius E, Annersten H, Jönsson S (1996) *In situ* $^{57}$Fe Mössbauer spectroscopy of iron and olivine at high pressure and temperature. *In* MD Dyar, CA McCammon, M Schaeffer (eds) Mineral Spectroscopy: A Tribute to Roger G. Burns, Vol 5. Geochemical Society, USA, p 255-260

Hawthorne FC (1988) Mössbauer spectroscopy. *In* FC Hawthorne (ed) Spectroscopic Methods in Mineralogy and Geology. Rev Mineral 18:255-340

Hearne GR, Pasternak MP, Taylor RD (1994) $^{57}$Fe Mössbauer spectroscopy in a diamond-anvil cell at variable high pressures and cryogenic temperatures. Rev Sci Instrum 65:3787-3792

Ingalls R (1964) Electric-field gradient tensor in ferrous compounds. Phys Rev 133:A787-A795

Johnson CE (1989) The Mössbauer effect and magnetic phase transitions. Hyper Inter 49:19-42

Kolk B (1984) Studies of dynamical properties of solids with the Mössbauer effect. *In* GK Horton, AA Maradudin (eds) Dynamical Properties of Solids, Vol 5. North Holland, Amsterdam, p 3-328

Kolk B, Bleloch AL, Hall DB, Zheng Y, Patton-Hall KE (1985) High-temperature Mössbauer-effect measurements with a precision furnace. Rev Sci Instrum 56:1597-1603

Kruger MB, Jeanloz R, Pasternak MP, Taylor RD, Snyder BS, Stacy AM, Bohlen SR (1992) Antiferromagnetism in Pressure-Amorphized $Fe_2SiO_4$. Science 255:703-705

Lauterbach S, McCammon CA, van Aken P, Langenhorst F, Seifert F (2000) Mössbauer and ELNES spectroscopy of $(Mg,Fe)(Si,Al)O_3$ perovskite: A highly oxidised component of the lower mantle. Contrib Mineral Petrol 138:17-26

Maddock AG (1985) Mössbauer spectroscopy in mineral chemistry. *In* FJ Berry, DJ Vaughan (eds) Chemical Bonding and Spectroscopy in Mineral Chemistry. Chapman and Hall, London, p 141-208

Margulies S, Ehrman JR (1961) Transmission and line broadening of resonance radiation incident on a resonance absorber. Nucl Instr Meth 12:131-137

McCammon CA (1994) A Mössbauer milliprobe: Practical considerations. Hyper Inter 92:1235-1239

McCammon CA, Price DC (1985) Mössbauer spectra of $Fe_xO$ ($x > 0.95$). Phys Chem Min 11:250-254

McCammon CA, Tennant C (1996) High-pressure Mössbauer study of synthetic clinoferrosilite, $FeSiO_3$. *In* MD Dyar, CA McCammon, M Schaeffer (eds) Mineral Spectroscopy: A Tribute to Roger G. Burns, Vol 5. Geochemical Society, USA, p 281-288

McCammon CA, Chaskar V, Richards GG (1991) A technique for spatially resolved Mössbauer spectroscopy applied to quenched metallurgical slags. Meas Sci Technol 2:657-662

McCammon CA, Becerro AI, Langenhorst F, Angel R, Marion S, Seifert F (2000) Short-range ordering of oxygen vacancies in $CaFe_xTi_{1-x}O_{3-x/2}$ perovskites ($0 \le x \le 0.4$). J Phys: Cond Matt 12:2969-2984

Morrish AH (1965) The physical properties of magnetism. John Wiley and Sons, Inc., New York, p 262-264

Mössbauer RL (1958a) Kernresonanzfluoresent von Gammastrahlung in $Ir^{191}$. Z Phys 151:124-143
Mössbauer RL (1958b) Kernresonanzfluoresent von Gammastrahlung in $Ir^{191}$. Naturwiss 45:538-539
Mössbauer RL, Wiedemann WH (1960) Kernresonanzabsorption nicht Doppler-verbreiterter Gammastrahlung in $Re^{187}$. Z Phys 159:33-48
Nikolov O, Hall I, Barilo SN, Mukhin AA (1996) Field-induced reorientations in $TbFeO_3$ at 4.2 K. J Magn Magn Mater 152:75-85
Nolle G, Ullrich H, Muller JB, Hesse J (1983) A microprocessor controlled spectrometer for thermal scan Mössbauer spectroscopy. Nucl Instr Meth Phys Res 207:459-463
Nomura K, Ujihira Y, Vertes A (1996) Applications of conversion electron Mössbauer spectrometry (CEMS). J Radioanal Nucl Chem 202:103-199
Pasternak MP, Taylor RD (1996) High pressure Mössbauer spectroscopy: The second generation. *In* GJ Long, F Grandjean (eds) Mössbauer Spectroscopy Applied to Magnetism and Materials Science, Vol. 2. Plenum Press, New York and London, p 167-205
Pasternak MP, Taylor RD, Jeanloz R, Li X, Nguyen JH, McCammon CA (1997) High pressure collapse of magnetism in $Fe_{0.94}O$; Mössbauer spectroscopy beyond 100 GPa. Phys Rev Lett 79:5046-5049
Pasternak MP, Rozenberg GR, Machavariani GY, Naaman O, Taylor RD, Jeanloz R (1999) Breakdown of the Mott-Hubbard state in $Fe_2O_3$: A first order insulator-metal transition with collapse of magnetism at 50 GPa. Phys Rev Lett 82:4663-4666
Perkins HK, Hazony Y (1972) Temperature-dependent crystal field and charge density: Mössbauer studies of $FeF_2$, $KFeF_3$, $FeCl_2$, and $FeF_3$. Phys Rev B 5:7-18
Ping JY, Rancourt DG (1992) Thickness effects with intrinsically broad absorption lines. Hyper Inter 71:1433-1436
Pound RV, Rebka Jr. JA (1960) Variation with temperature of the energy of recoil-free gamma rays from solids. Phys Rev Lett 4:274-277
Preston RS (1978) Isomer shift at phase transitions. *In* GK Shenoy, FE Wagner (eds) Mössbauer Isomer Shifts. North-Holland Publishing Co., Amsterdam, p 281-316
Rancourt DG (1989) Accurate site populations from Mössbauer spectroscopy. Nucl Instr Meth Phys Res B44:199-210
Rancourt DG, Klingelhöfer G (1994) Possibility of a Mössbauer resonant-electron microscope. Fourth Seeheim Workshop on Mössbauer Spectroscopy, p 129
Rancourt DG, Mcdonald AM, Lalonde AE, Ping JY (1993) Mössbauer absorber thicknesses for accurate site populations in Fe-bearing minerals. Am Mineral 78:1-7
Riedel E, Karl R (1980) Mössbauer studies of thiospinels. I. The system $FeCr_2S_4$-$FeRh_2S_4$. J Sol State Chem 35:77-82
Rozenberg GR, Machavariani GY, Pasternak MP, Milner AP, Hearne GR, Taylor RD, Adler P (1999) Pressure-induced metallization of the perovskite $Sr_3Fe_2O_7$. Phys Stat Sol B 211:351-357
Ruby SL (1973) Mössbauer studies of acqueous liquids and glasses. *In* SG Cohen, M Pasternak (eds) Perspectives in Mössbauer Spectroscopy. Plenum Press, New York-London, p 181-194
Ruffer R, Chumakov AI (1996) Nuclear Resonance Beamline at ESRF. Hyper Inter 97/98:589-604
Seifert F (1983) Mössbauer line broadening in aluminous orthopyroxenes: Evidence for next nearest neighbors interactions and short-range order. Neues Jahrbuch Miner Abh 148:141-162
Seifert F (1990) Phase transformation in minerals studied by $^{57}Fe$ Mössbauer spectroscopy. *In* A Mottana, F Burragato (eds) Absorption Spectroscopy in Mineralogy. Elsevier, Amsterdam, p 145-170
Shenoy GK (1973) Mössbauer effect studies of phase transitions. *In* SG Cohen, M Pasternak (eds) Perspectives in Mössbauer Spectroscopy. Plenum Press, New York-London, p 141-169
Skogby H, Annersten H, Domeneghetti MC, Molin GM, Tazzoli V (1992) Iron distribution in orthopyroxene: A comparison of Mössbauer spectroscopy and x-ray refinement results. Eur J Mineral 4:441-452
Takano M, Nakanishi N, Takeda Y, Naka S, Takada T (1977) Charge disproportionation in $CaFeO_3$ studied with the Mössbauer effect. Mater Res Bull 12:923-928
Takano M, Nasu S, Abe T, Yamamoto K, Endo S, Takeda Y, Goodenough JB (1991) Pressure-induced high-spin to low-spin transition in $CaFeO_3$. Phys Rev Lett 67:3267-3270
Virgo D, Hafner SS (1969) $Fe^{2+}$,Mg order-disorder in heated orthopyroxenes. Mineral Soc Am Spec Paper 2:67-81
Wang Z, Cooney TF, Sharma SK (1993) High temperature structural investigation of $Na_2O{\cdot}0.5Fe_2O_3{\cdot}3SiO_2$ and $Na_2O{\cdot}FeO{\cdot}3SiO_2$ melts and glasses. Contrib Mineral Petrol 115:112-122
Weiss P (1906) La variation du ferromagnétisme avec la température. Comptes Rendus des Séances de L'Académie des Sciences 143:1136-1139
Wertheim GK (1973) Phase transitions in Mössbauer spectroscopy. *In* HK Henisch, R Roy (eds) Phase Transition-1973. Pergamon Press, New York, p 235-242

Williams JM (1975) The Mössbauer effect and its applications at very low temperatures. Cryogenics:307-322

Williamson DL (1978) Influence of pressure on isomer shifts. *In* GK Shenoy, FE Wagner (eds) Mössbauer Isomer Shifts. North-Holland Publishing Co., Amsterdam, p 317-360

Woodland AB, Angel RJ (1997) Reversal of the orthoferrosilite-High-P clinoferrosilite transition, a phase diagram for $FeSiO_3$ and implications for the mineralogy of the Earth's upper mantle. Eur J Mineral 9:245-254

Woodland AB, McCammon CA, Angel RJ (1997) Intersite partitioning of Mg and Fe in Ca-free high-pressure C2/c clinopyroxene. Am Mineral 82:923-930

Zou GT, Mao HK, Bell PM, Virgo D (1980) High pressure experiments on the iron oxide wüstite. Carnegie Inst Washington Yrbk 79:374-376

## APPENDIX

### Worked example: Incommensurate-normal phase transformation in Fe-doped åkermanite

***Introduction.*** Fe-åkermanite, $Ca_2(Fe,Mg)Si_2O_7$, crystallises in the melilite structure, which consists of $Si_2O_7$ dimers connected via tetrahedrally coordinated $Mg^{2+}/Fe^{2+}$ sites to form a sheet-like arrangement. At high temperature it exhibits a normal (N) structure with space group $P\bar{4}2_1m$, which transforms reversibly to an incommensurate (IC) structure with decreasing temperature. Theoretical analysis indicates that there are two component structures within the modulation with symmetries $P\bar{4}$ and $P2_12_12$ (McConnell 1999), which correlates with earlier work by Seifert et al. (1987) who showed that Mössbauer spectra of the IC structure showed two quadrupole doublets. Since Mössbauer spectroscopy is one of the few techniques able to distinguish between the component structures in the IC structure, McConnell et al. (2000) undertook a study using *in situ* Mössbauer spectroscopy at variable temperature and at high pressure to further characterise the IC structure and the IC-N phase transformation in Fe-åkermanite.

***Sample preparation and data collection.*** In order to study the phase transformation in a sample close to the $Ca_2MgSi_2O_7$ endmember, the minimum amount of enriched $^{57}Fe$ required to obtain an adequate signal must be calculated. First, the optimum thickness for 90% $^{57}Fe$ enrichment was determined using Long et al. (1983) for a series of Fe-doped åkermanites, $Ca_2Fe_xMg_{1-x}Si_2O_7$. The results are listed in Table A1 in terms of the dimensionless thickness (Eq. 12, this Chapter), and show that addition of 0.005 $^{57}Fe$ atoms p.f.u. would be sufficient to obtain an adequate signal for conventional transmission measurements (a dimensionless thickness of 2.6 corresponds to an

**Table A1.** Optimum Fe concentration for $Ca_2Fe_xMg_{1-x}Si_2O_7$ Fe-åkermanite based on Long et al. (1983) and $^{57}Fe$ enrichment of 90%

| *x* | *Optimum Fe concentration (mg $^{57}Fe/cm^2$)* | *Dimensionless thickness* |
|---|---|---|
| 0.005 | 0.15 | 2.6 |
| 0.01 | 0.30 | 5.1 |
| 0.02 | 0.54 | 10.1 |
| 0.03 | 0.88 | 15.0 |
| 0.04 | 1.16 | 19.8 |
| 0.05 | 1.44 | 24.5 |

unenriched Fe concentration of 7 mg Fe/cm$^2$, which is sufficient to give an adequate signal:noise ratio). The optimum thickness calculation assumes that the physical thickness of the absorber is unrestricted, i.e. that a sufficient amount of sample can be added to the absorber in order to achieve the desired iron concentration. For high pressure experiments, however, this is generally not possible, since the physical thickness of the absorber is constrained by the gasket to be no more than approximately 100 μm. The calculation of optimum thickness was then repeated using this constraint, showing that a concentration corresponding to $x$ = 0.03 would be needed to give an unenriched Fe concentration near 7 mg Fe/cm$^2$ for a 100 μm thick absorber.

Mössbauer spectra were collected as a function of temperature at room pressure, and as a function of pressure at room temperature. This was accomplished using a continuous flow cryostat for temperatures from 4.2 to 293 K, a vacuum furnace for temperatures from 293 to 425 K, and a diamond anvil cell for pressures from 0 to 5.3 GPa. Further details are given in McConnell et al. (2000).

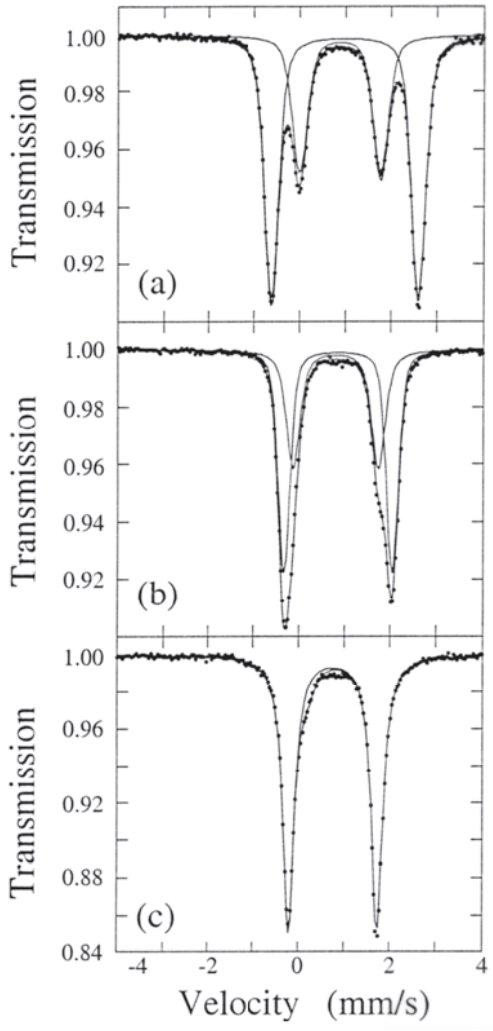


**Figure A1**. Mössbauer spectra of $Ca_2Fe_xMg_{1-x}Si_2O_7$ Fe-åkermanite at atmospheric pressure and (a) 4.2 K; (b) 293 K; and (c) 400 K. The outer two lines refer to the $P\bar{4}$ symmetry while the inner two lines refer to the $P2_12_12$ symmetry. The small amount of additional absorption in the spectrum recorded at 400 K is due to impurities in the furnace windows (data taken from McConnell et al. 2000).

***Fitting models.*** Visually the spectra consist of two quadrupole doublets, where resolution improves with decreasing temperature. Above the IC-N transformation there is only one quadrupole doublet (Fig. A1). A general approach to fitting is to select the simplest model that is physically realistic, yet provides a good statistical fit to the experimental data. The conventional constraint of equal component areas of the quadrupole doublets was applied, since effects such as preferred orientation or anisotropic recoil-free fraction are not expected to be present. Component linewidths were also assumed to be equal, despite evidence at 4.2 K for a slight asymmetry in the single N-structure doublet. Doublet separation is not sufficient at higher temperatures to enable a unique determination of the asymmetry, but fortunately neglect of the asymmetry has a negligible effect on the line positions. Nine variables were fit to each spectrum: the baseline and four variables for each doublet (linewidth, area, centre shift and quadrupole splitting). For spectra recorded at 4.2 and 80 K, fits using Lorentzian lineshapes gave large residuals, so Voigt lineshapes were used instead. Voigt lines represent a Gaussian distribution of Lorentzian lines, and are expected when there are variations in the iron environment for a particular site,

such as for solid solutions. These added an additional variable per doublet, the Gaussian standard deviation, and an F test was used (e.g. Bevington 1969) to confirm that addition of these variables was statistically significant to better than the 99% level. This was not the case for spectra recorded at higher temperatures, and for all spectra recorded at high pressure, so those were fit to Lorentzian lineshapes only.

***Transition temperature and pressure.*** The IC-N transformation is recognised from the Mössbauer spectra as the point at which the two subspectra collapse to a single quadrupole doublet. This point is difficult to recognise from the two-doublet fits, however, due to the large line overlap just below the transition. A different approach was therefore used to determine the IC-N phase transformation point. Following the method of Seifert et al. (1987), two singlets were fit to the Mössbauer spectra, meaning that the high-velocity components of both subspectra were fit to a single line, and likewise for the low-velocity components. While the singlets do not provide a good statistical fit to the data in the IC structure region, their linewidths provide a measure of the splitting between the two subspectra. The linewidths are large at low temperature where the two subspectra are well resolved, and smaller at high temperature where subspectra overlap more (Fig. A1). The difference between the two singlet linewidths was used to monitor the approach to the IC-N phase transformation, where the transition point is seen as a discontinuity in the slope of linewidth difference versus temperature, and a break in the slope of linewidth difference versus pressure **(Fig. A2).** The transition temperature at room pressure is consistent with the linear trend shown by Seifert et al. (1987) as a function of iron composition, and the transition pressure at room temperature is consistent with the results from high-pressure X-ray diffraction reported by McConnell et al. (2000).

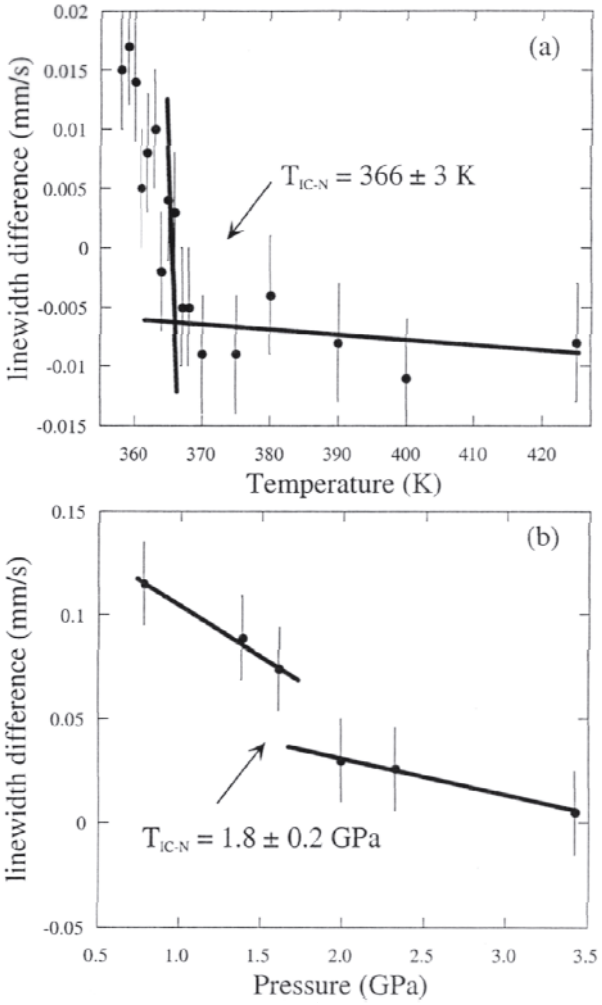


**Figure A2**. Variation of the difference in linewidth between high- and low-velocity components as a function of (a) temperature; and (b) pressure. The linewidths were determined based on a fit of two singlets to the Mössbauer spectra. The IC-N transition is recognised as either a discontinuity or a break in the slope in the variation near the transition.

***Application of the Debye model.*** The centre shift data collected at room pressure and variable temperature were fit to the Debye model (Eq. 2, this Chapter). The integral can be evaluated using a series approximation, where only a few terms of the series are needed needed to achieve an accuracy that exceeds the experimental one (Heberle 1971).

At low temperatures ($z = \Theta_M/T < 2.5$) the following expression approximates the integral:

$$D_3(z) = \int_0^z \frac{x^3}{e^x - 1} dx$$
$$\approx \frac{\pi^4}{15} + z^3 \ln\left(1 - e^{-z}\right) - 3e^{-z}\left(z^2 + 2z + 2\right) - \frac{3}{16} e^{-2z}\left(4z^2 + 4z + 2\right), \quad \text{(A1)}$$

while at high temperatures ($z = \Theta_M/T > 2.5$) the following expression is used:

$$D_3(z) = \int_0^z \frac{x^3}{e^x - 1} dx \approx \frac{z^3}{3}\left(1 - \frac{3}{8}z + \frac{z^2}{20} - \frac{z^4}{1680} + \frac{z^6}{90720}\right). \quad \text{(A2)}$$

The equation describing the variation of centre shift with temperature (Eq. 1, this Chapter) contains two adjustable parameters, $\Theta_M$ and $\delta_0$. Using a non-linear least squares method, the values of these parameters which best fit the data were determined (Table A2). The centre shift data together with the Debye model calculations are plotted in Figure A3.

**Table A2.** Best-fit Debye model parameters for $Ca_2Fe_{0.03}Mg_{0.97}Si_2O_7$ Fe-åkermanite derived from Mössbauer centre shift data

| | $\delta_0$ (mm/s) | $\Theta_M$ (K) |
|---|---|---|
| IC symmetry #1 $\rightarrow P\bar{4}$ | 1.101(3) | 340(18) |
| IC symmetry #2 $\rightarrow P2_12_12$ | 0.995(3) | 774(31) |
| N structure $P\bar{4}2_1m$ | .004(3) | 791(23) |

***Relative area.*** The relative areas of the quadrupole doublets are related to the relative abundance of each component, which can be estimated according to the thin absorber approximation (Eqn. 13, this Chapter) in cases where the approximation is valid. Rancourt et al. (1993) provide a means of estimating how closely the thin absorber approximation is satisfied for a given absorber based on the attenuation of spectral areas for individual lines (see Fig. 3 in their paper). McConnell et al. (2000) used an iron density in the high temperature experiments corresponding to an unenriched concentration of 5 mg Fe/cm$^2$, which is equivalent to a dimensionless effective thickness of 2.0. The attenuation of spectral

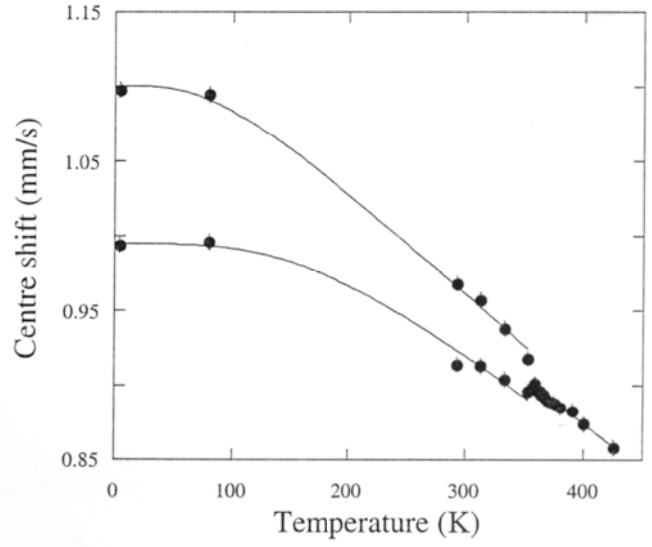


**Figure A3**. Variation of centre shift with temperature based on spectral fits incorporating two quadrupole doublets. The solid line represents the Debye model fit (Eqns. 1 and 2, this Chapter) to the centre shifts (data taken from McConnell et al. 2000).

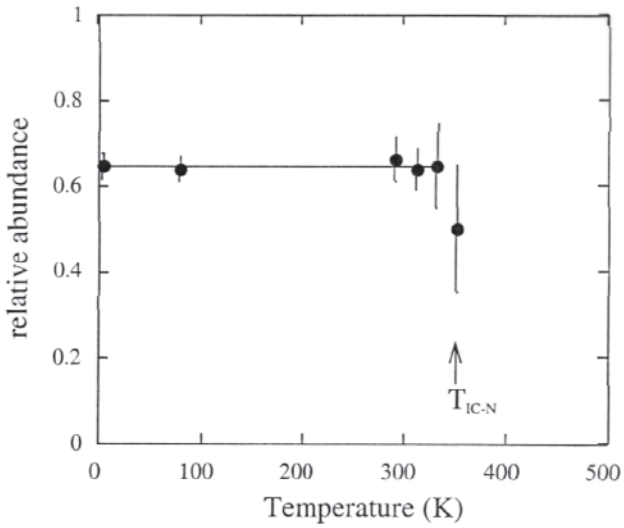


**Figure A4**. Relative abundance of the IC structure component with high quadrupole splitting (doublet #1) plot-ted as a function of temperature. The relative abundance was calculated from the relative areas as described in the text, and the solid line represents a constant *y*-axis value of 0.64.

areas increases as the relative abundance of the individual components becomes more different, so the maximum thickness effect can be estimated assuming the greatest possible difference in component abundances. The maximum abundance ratio is estimated to be 2:1, which implies effective thicknesses of 1.34 and 0.66 for the two components. The effective thickness is halved for each line of a quadrupole doublet, hence the relevant numbers for the *x*-axis in Figure 3 of Rancourt et al. (1993) are 0.67 and 0.33. The *y*-axis value for Figure 3 is calculated from $\Gamma_{obs} - 2\Gamma_0$, where the observed linewidth is 0.36 mm/s, which implies a *y*-axis value of 0.17 mm/s. This gives area attenuations of approximately 0.93 and 0.96 for the two components, which can be considered to lie close to the thin absorber approximation (Rancourt et al. 1993).

Another consideration for calculating relative abundances from the relative areas is the difference in recoil-free fractions corresponding to the specific sites. The Debye model allows recoil-free fractions to be estimated using Equation (15) (this Chapter), and combined with the results listed in Table A2, gives recoil-free fractions of the two components at 4.2 K of 0.91 and 0.96. This results in, at most, a 2% correction to the relative areas in order to obtain the relative abundances. The situation is different at room temperature, however, where recoil-free fractions of the two components are calculated to be 0.70 and 0.92, which results in a correction of more than 10%.

The relative abundance (determined as described above) of the component corresponding to doublet #1 is plotted in Figure A4. The relative abundance remains relatively constant within the IC structure stability region until just before the transition, where it apparently decreases to approximately 50%. This is consistent with theory that requires the abundance of the two components to be equal at the phase transformation (McConnell 1999).

***Interpretation.*** The Mössbauer spectra obtained for the IC structure in Fe-åkermanite comprise two and only two subspectra over the temperature range down to 4.2 K. In terms of the theoretical model (McConnell 1999), they may be identified with the two symmetries $P\bar{4}$ and $P2_12_12$. The former involves a simple rotation of the tetrahedral site with respect to the $Si_2O_7$ dimers and hence no change to the coordination environment, while the latter involves an orthorhombic site distortion. The quadrupole doublets observed in the IC structure spectrum may be characterised as follows:

Doublet #1 – high $\Delta E_Q$, large decrease in $\Delta E_Q$ with increasing temperature, normal $\Theta_M$
Doublet #2– low $\Delta E_Q$, small increase in $\Delta E_Q$ with increasing temperature, anomalous $\Theta_M$

Doublet #1 may be assigned unambiguously to $P\bar{4}$ symmetry, since the hyperfine parameters follow the expected behaviour for $Fe^{2+}$ in a relatively undistorted tetrahedral site. The high value of quadrupole splitting indicates a high valence contribution, and displays the expected temperature variation for tetrahedral environments (Gibb 1968). The characteristic Mössbauer temperature $\Theta_M$ is in the range expected for $Fe^{2+}$ (De Grave and Van Alboom 1991).

Doublet #2 may be assigned unambiguously to $P2_12_12$ symmetry. The small quadrupole splitting indicates a high lattice contribution, which is consistent with the small temperature dependence of the quadrupole splitting (Fig. 4, this Chapter). The anomalously high value of $\Theta_M$ is likely related to constraints on lattice vibrations imposed by symmetry. Similar constraints evidently exist also in the normal structure, since the value of $\Theta_M$ is comparable.

***Summary.*** Mössbauer spectroscopy confirms results from the theoretical analysis of incommensurate structures using full space group theory that the IC structure of melilite comprises two (and only two) component structures (McConnell 1999). Mössbauer spectra of Fe-åkermanite contain two quadrupole doublets at low temperature and pressure (IC structure) and one quadrupole doublet at high temperature and pressure (N structure). Transition temperatures and pressures, as well as parameters relating to the structures of the IC and N structures, were determined from *in situ* Mössbauer measurements. The characteristic Mössbauer temperatures of the N structure and the $P2_12_12$ component of the IC structure are anomalous, which is likely related to symmetry-imposed constraints on lattice vibrations. Quadrupole splitting values and their temperature dependence are consistent with the symmetry-imposed distortions of the two components of the IC structure. The relative abundance of the two components appears to be equal at the transition temperature, as required by theory, while at low temperatures the relative abundance of the $P\bar{4}$ symmetry is larger, indicating that it is the favoured configuration.

## APPENDIX REFERENCES

Bevington PR (1969) Data Reduction and Error Analysis for the Physical Sciences. McGraw-Hill, New York

De Grave E, Van Alboom A (1991) Evaluation of ferrous and ferric Mössbauer fractions. Phys Chem Min 18:337-342

Gibb TC (1968) Estimation of ligand-field parameters from Mössbauer spectra. J Chem Soc A:1439-1444

Heberle J (1971) The Debye integrals, the thermal shift and the Mössbauer fraction. *In* IJ Gruverman (ed) Mössbauer Effect Methodology, Vol 7. Plenum Press, New York, p 299-308

Long GL, Cranshaw TE, Longworth G (1983) The ideal Mössbauer effect absorber thickness. Möss Effect Ref Data J 6:42-49

McConnell JDC (1999) The analysis of incommensurate structures in terms of full space group theory, and the application of the method to melilite. Z Krist 214:457-464

McConnell JDC, McCammon CA, Angel RJ, Seifert F (2000) The nature of the incommensurate structure in åkermanite, $Ca_2MgSi_2O_7$, and the character of its transformation from the normal structure. Z Krist (in press)

Rancourt DG, Mcdonald AM, Lalonde AE, Ping JY (1993) Mössbauer absorber thicknesses for accurate site populations in Fe-bearing minerals. Am Mineral 78:1-7

Seifert F, Czank M, Simons B, Schmahl W (1987) A commensurate-incommensurate phase transition in iron-bearing Åkermanites. Phys Chem Min 14:26-35